Supporting Information

Exclusively Generating Superoxide Radical by Porous Aromatic Frameworks for Fast Photocatalytic Decontamination of Mustard Gas Simulant in Room Air

Jian Song,[†] Hengtao Lei,[†] Yuhui Zhai, Zilong Dou, Yongyue Ding, Xueyan Han, Fengchao Cui, Yuyang Tian* and Guangshan Zhu*

Key Laboratory of Polyoxometalate and Reticular Material Chemistry of Ministry of Education, Faculty of Chemistry, Northeast Normal University,

Changchun, Jilin 130024, China.

E-mail: tianyy100@nenu.edu.cn; zhugs@nenu.edu.cn.

Table of Contents

1. General Information

1.1 Materials and Reagents

All the reagents were purchased from commercial sources without further purification.

1.2 Instrumentation

FT-IR was performed on a Nicolet-410 FT-IR spectrophotometer. Scanning electron microscopy (SEM) was performed on a HITACHI SU8010 microscope. The ^{13}C MAS solid-state NMR spectra of PAF-68 were obtained using a Bruker Avance III model 400 MHz NMR spectrometer at a MAS rate of 5 kHz. N_2-adsorption isotherms were recorded at 77 K by an Autosorb iQ2 adsorptometer, Quantachrome Instruments. Specific surface areas were obtained by using the Brunauer-Emmet-Teller (BET) model, and pore size distributions were evaluated by the nonlocal density functional theory (NLDFT) model. Thermogravimetric analysis (TGA) was measured on a Mettler Toledo thermal analyzer in the temperature range 30–800℃ with a heating rate of 10℃ min^{-1} under a flow of air. The UV-vis diffuse reflectance spectra were measured using a Cary 500 UV-Vis-NIR spectrophotometer and the solid-state UV-vis diffuse reflectance spectra were measured using a Cary 7000 UV-Vis-NIR spectrophotometer with $BaSO_4$ as the reference. XPS was implemented on a Thermo Scientific K-Alpha. Electron paramagnetic resonances (EPR) were recorded on a Bruker EMXPLUS electron paramagnetic resonance spectrometer at liquid-nitrogen temperature in the absence and presence of Xe light irradiation. The temperature-dependent PL measurements were measured by Edinburgh-FLS1000 fluorescence and phosphorescence spectrometer. The time-resolved fluorescence spectra were obtained on helios of ultrafast systems. With the time-resolved fluorescence spectra were recorded with 470 nm excitation, while other spectra were obtained with 522 nm excitation. ^{1}H NMR and ^{13}C NMR spectra were recorded on a Bruker Avance NEO 500 instrument at 500 MHz.

2. Methods

2.1 Synthesis of PAF-68

A 100 mL two-neck round bottom flask was charged with meso-Tetra (p-bromophenyl) porphine (TBPP, 0.250 g, 0.269 mmol) under a nitrogen atmosphere. Then, Tris(4-ethynylphenyl) amine (EPA, 0.114 g, 0.358 mmol), tetrakis(triphenylphosphine) palladium (0) (0.040 g, 0.04 mmol), copper(I) iodide (0.015 g, 0.075 mmol), 15 mL DMF and 15 mL triethylamine were quickly added under continuous nitrogen flow, and degassed by three freeze–pump–thaw cycles. The mixture was stirred and heated at 100℃ for 48 hours. After cooling to room temperature, the product was filtered and washed with 3 mol L^{-1} HCl (120 mL*2), H_2O (120 mL*2), EtOH (120

mL*2) and CH_2Cl_2 (120 mL*2) to remove the catalyst and unconsumed reactants. The product was further purified by Soxhlet extraction with THF for 24 h. Lastly the product was dried under vacuum at 100℃ for 8 h to give a purple powder (208 mg with 92% yields).

2.2 Detection of $\cdot O_2^-$ Generation

TMB

TMB 12.9 mg of 3,3',5,5'-Tetramethylbenzidine (TMB) dispersed 2.5 mL of EtOH and 5 mL of HAc/NaAc buffer solution (1:1, 0.1 M). PAF-68 (1.3 mg, 1.29 μmoL) was added to the mixed solution and irradiated under a Xe lamp with a light intensity of 0.5 $W \cdot cm^{-2}$. The ultraviolet visible absorption chart recording function on a Cary 500 UV-Vis-NIR was used to collect samples at different time intervals. In order to verify the specificity of reactive oxygen species, 1,4-Benzochinon (13 mg) for $\bullet O_2^-$, tert-butanol (13 μL) for •OH, catalase (13 μL) for H_2O_2, carotene (13 mg) for $^1O_2$ were added to a TMB solution before photoirradiation.

EPR

the 5,5-Dimethyl-1-pyrroline-oxide (DMPO) was utilized as a trapping agent to detect the EPR signals of $\bullet O_2^-$ and •OH. 2,2,6,6-Tetramethyl-4-piperidone (4-oxo-TMP) was utilized as a trapping agent to detect the EPR signals of $^1O_2$.

2.3 Computational Details

Ground-state geometry optimization of PAF68 was carried out with the M062x[10]/6-311G(d,p) level of theory. All excited geometry, including S1, T1 and T2 states were optimized with the TD-M062x[1]/6-311G(d,p) level of theory. Based on the geometry structures of every state (S0, S1, T1 and T2), the singlet and triplet excitation energies were calculated with the same level of theory. The solvent effects were considered using SMD[11] model with the implicit solvent of methanol. All quantum chemical calculations were performed with the Gaussian 16 programs[12].

2.4 Arrhenium formula simulation of the binding energy.

In the temperature-dependent steady-state photoluminescence measurement, we have

$$I(T) = \frac{I_0}{(1 + Ae^{-\frac{E_b}{KT}})}$$

in which I_0 is the intensity at 0 K, Eb the exciton binding energy and k the Boltzmann constant. After fitting I(T), we can determine Eb. The thermal dissociation ratio (T.D.R.) is

$$T.D.R = e^{-\frac{E_b}{KT}}$$

2.5 Photocatalytic CEES degradation experiment using PAF-68

The Xe lamp was adjusted to a light intensity of 0.5 W·cm^{-2}. PAF-68 (1.3 mg, 1.29 μmoL porphyrin unit) were dispersed in 5 mL of CD_3OD and placed in a quartz reactor and the mixture was sonicated for 2 min. The reactor was purged with O_2/Air/mixed gas for 10 min, 15 μL (129 μmol) of CEES was added to the quartz reactor with a micro syringe. Then, the reactor was exposed to simulated solar light and monitored by NMR measurement.

To study the effect of humidity on the catalytic performance of PAF-68, water vapor was added to the gas mixture flow at 3.169 kPa.

2.6 Reusability test

After the photocatalytic reaction, the catalyst was separated by filtration and washed thrice with CH_3OH (10 mL). The powder was dried under vacuum. Then, the powder was added to CD_3OD in a quartz reactor. After bringing in the required gas and activation under simulated solar light for 10 minutes，fresh CEES (15 μL) was added to the mixture, and the resultant mixture was directly used for the next catalytic cycle.

3. Supplemental Figures and Tables

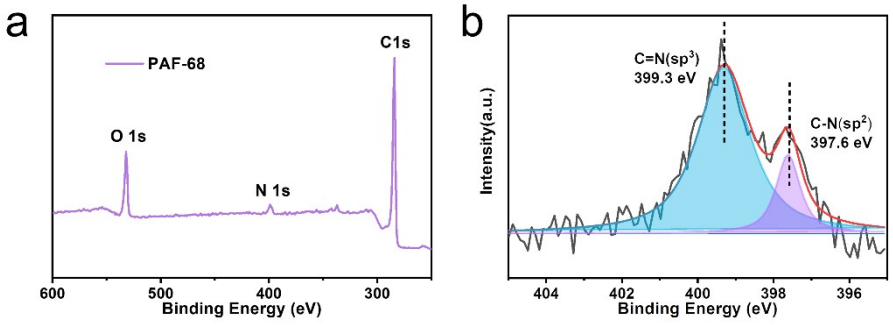

Fig. S1. (a) XPS full spectrum of PAF-68; (b) High-resolution N 1s XPS spectra of PAF-68.

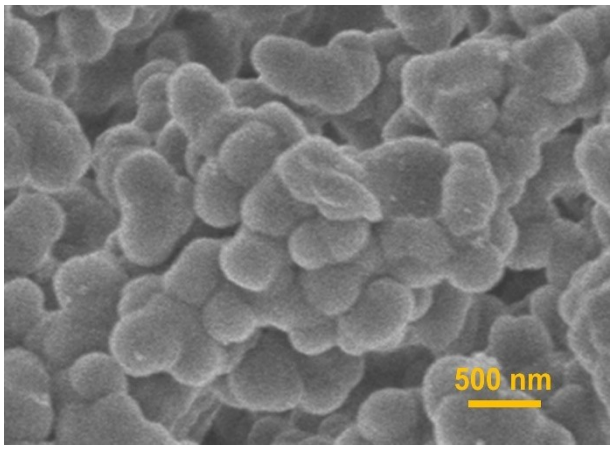

Fig. S2. SEM images of PAF-68. Scale bar: 500 nm.

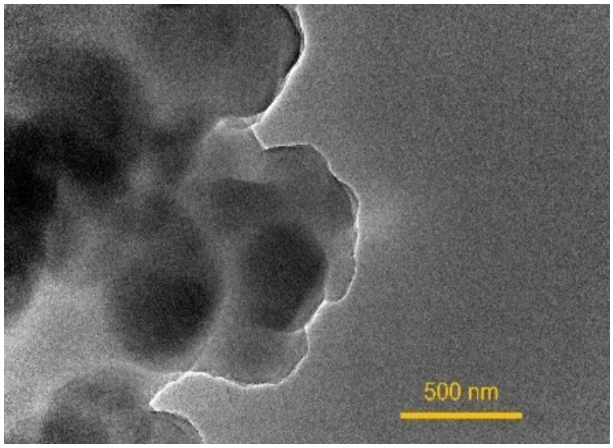

Fig. S3. TEM images of PAF-68. Scale bar: 500 nm.

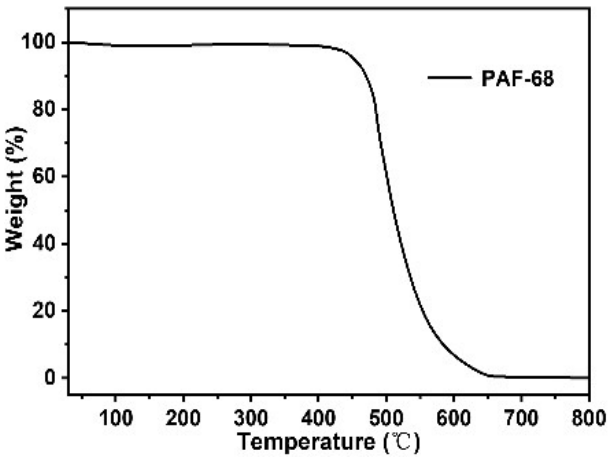

Fig. S4. TGA plot of PAF-68.

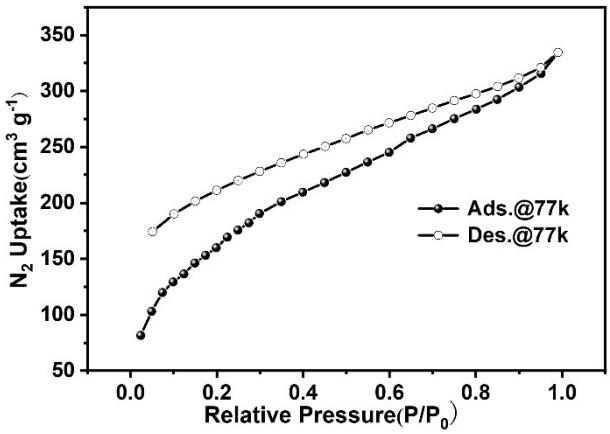

Fig. S5. Nitrogen-sorption isotherm curves of PAF-68 after stirring in 3M HCl for 48 hours. The BET surface area of treated PAF-68 was estimated to be 534 m^2 g^{-1}.

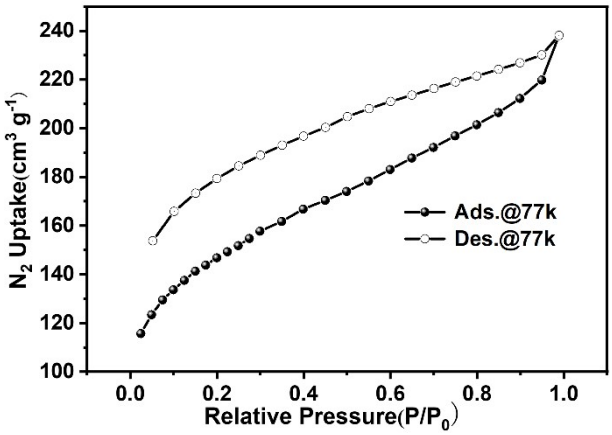

Fig. S6. Nitrogen-sorption isotherm curves of PAF-68 after stirring in 6M KOH for 48 hours. The BET surface area of treated PAF-68 was estimated to be 503 m^2 g^{-1}.

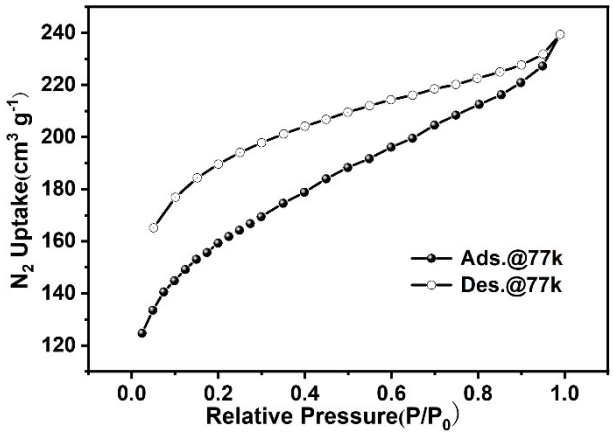

Fig. S7. Nitrogen-sorption isotherm curves of PAF-68 after stirring in commonly used organic solvents including tetrahydrofuran, methanol, dichloromethane, ethanol, and acetone for 24 hours. The BET surface area of treated PAF-68 was estimated to be 513 m^2 g^{-1}.

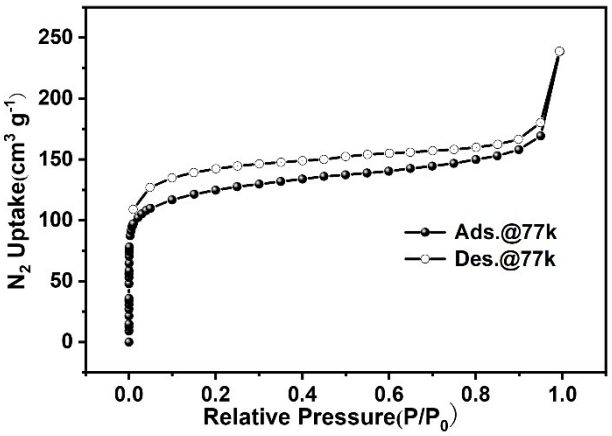

Fig. S8. Nitrogen-sorption isotherm curves of PAF-68 after being in normal room air for over a year. The BET surface area of treated PAF-68 was estimated to be 496 m^2 g^{-1}.

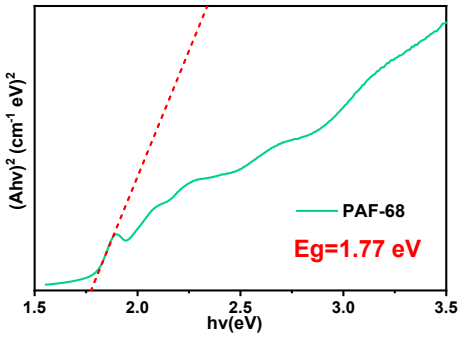

Fig. S9. Solid state diffuse reflectance spectrum determined optical energy gaps of PAF-68.

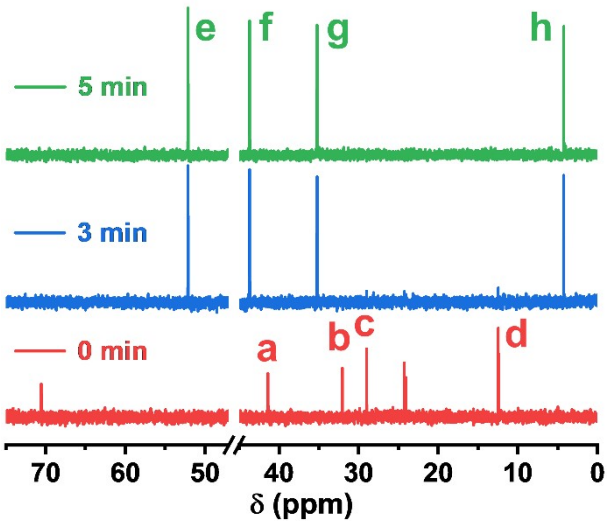

Fig. S10. ^{13}C NMR spectra measured 0 min, 3min and 5 min before and after photooxidation under pure oxygen.

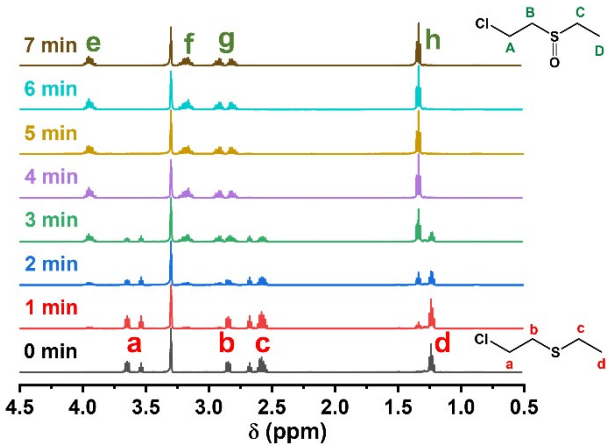

Fig. S11. ^{1}H NMR spectra measured before and after photooxidation in pure oxygen.

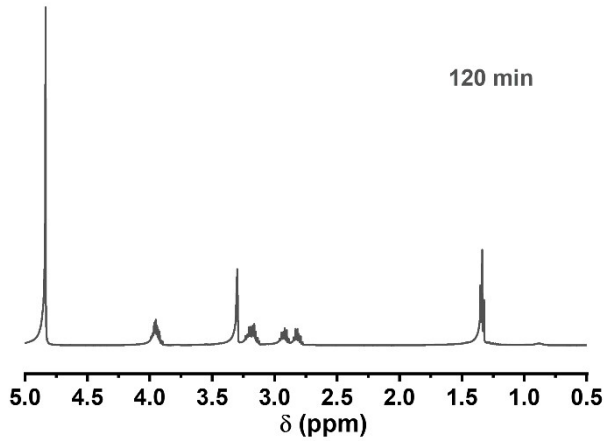

Fig. S12. ^{1}H NMR spectra measured 120 min after photooxidation in pure oxygen.

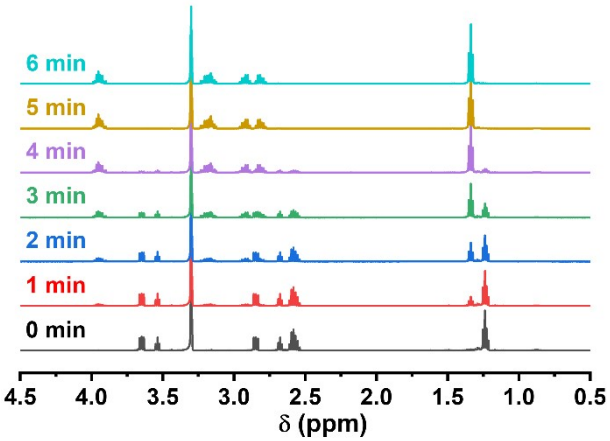

Fig. S13. ^{1}H NMR spectra measured before and after photooxidation in humidity oxygen.

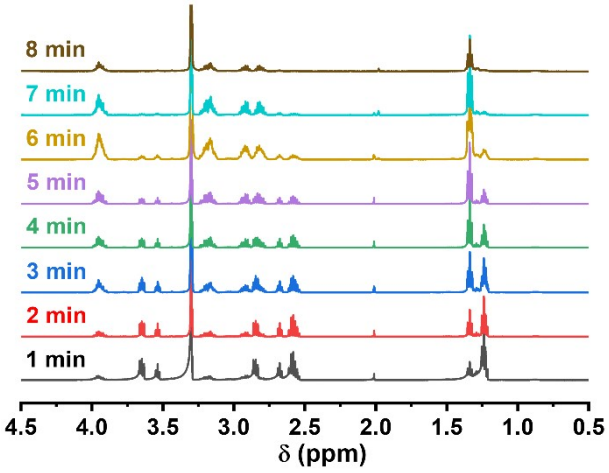

Fig. S14. ^{1}H NMR spectra measured after photooxidation in imitated air (N_2/O_2, v/v= 80,20).

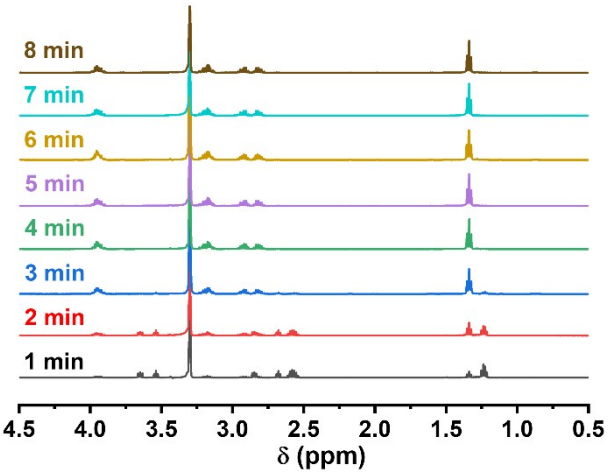

Fig. S15. ^{1}H NMR spectra measured after photooxidation in humidity imitated air (N_2/O_2, v/v= 80,20).

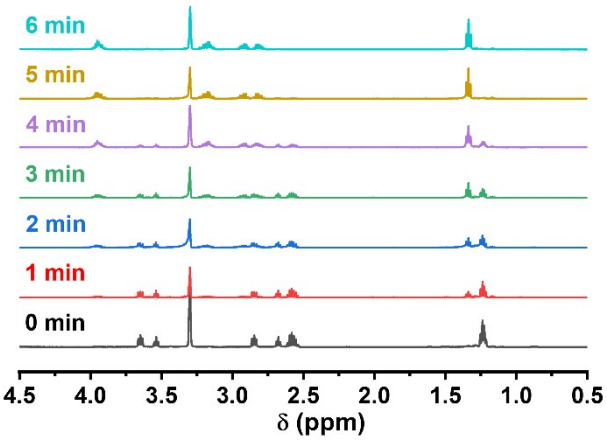

Fig. S16. ^{1}H NMR spectra measured before and after photooxidation in real room air.

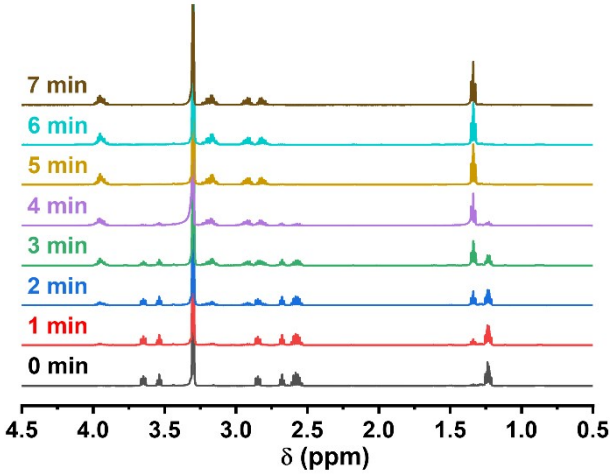

Fig. S17. ^{1}H NMR spectra measured before and after photooxidation in humidity real room air.

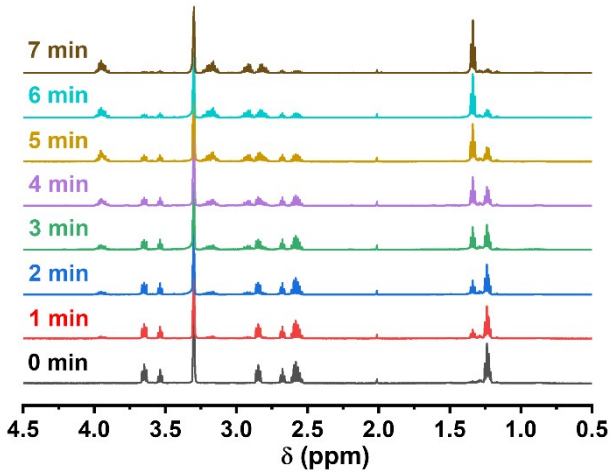

Fig. S18. ^{1}H NMR spectra measured before and after photooxidation in an atmosphere with extremely low-oxygen condition (N_2/O_2, v/v= 98,2).

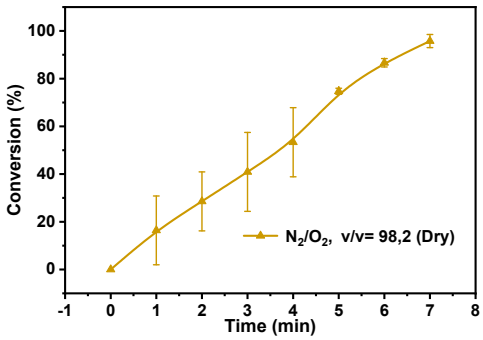

Fig. S19. Conversion of CEES in the presence of PAF-68 in an atmosphere with extremely low-oxygen condition (N_2/O_2, v/v= 98,2).

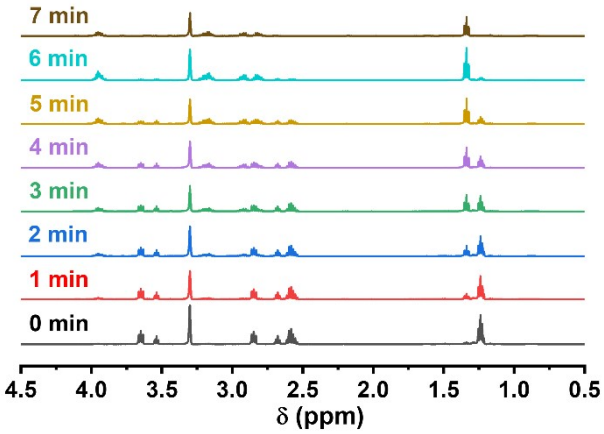

Fig. S20. ^{1}H NMR spectra measured before and after photooxidation in a humidity atmosphere with extremely low-oxygen condition (N_2/O_2, v/v= 98,2).

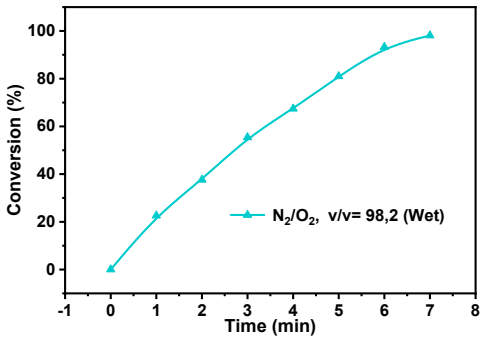

Fig. S21. Conversion of CEES in the presence of PAF-68 in a humidity atmosphere with extremely low-oxygen condition (N_2/O_2, v/v= 98,2).

Table S1. Comparison of the ability for degrading CEES by using POP photosensitizers with pure oxygen and air.

catalyst	catalyst loading	photosensitizer	oxidant	conversion efficiency	LED type and Power densities ($mWcm^{-2}$)	reference
PCN-222	0.5%	porphyrin	O_2	$t_{1/2}$ = 13 min $t_{1/2}$ = 26 min $t_{1/2}$ = 33 min	blue (325) white (310) red (160)	1
Ag12TpyP	1%	porphyrin	O_2 Air	$t_{1/2}$ = 1.5 min $t_{1/2}$ = 6 min	White (80)	2
Fc-based CMPs	10 mg	TEB TPE	O_2	75 min = 100%	Xe 1 W/cm^2 (simulated	3

		pyrene			solar light)	
CzBSe-CMP	2.0 mg	carbazole	O_2	1 h > 99%	LED (blue)	4
Py-Td-COF	5 mg	pyrene	O_2	1 h = 100%	Xe	5
Al-PMOF	0.2%	porphyrin	O_2	$t_{1/2}$ = 4 min	LED (blue)	6
H-BDP-POP I-BDP-POP Br-BDP-POP	1%	BODIPY	O_2	$t_{1/2}$ = 17 min $t_{1/2}$ = 3 min $t_{1/2}$ = 3 min	green (450)	7
M-TCPP-La	1%	porphyrin	O_2 Air	$t_{1/2}$ = 2.5 min $t_{1/2}$ = 10 min	LED (blue)	8
Por-Aminal-COF	0.25%	porphyrin	O_2	$t_{1/2}$ = 5 min	White (80)	9
PAF-68	**1%**	**porphyrin**	**O_2** **Air**	**$t_{1/2}$ = 1.5 min** **$t_{1/2}$ = 1.9 min**	**Xe 0.5 W/cm^{-2} (simulated solar light)**	**Our work**

Compared with previously reported POP photocatalyst, PAF-68, a class of porous materials entirely constructed from organic building units, where the building units are linked via stable carbon-carbon covalent bonds. Possessing numerous accessible internal surfaces, a stable framework, and sub-nanometer scaled pores during the catalytic reaction. Moreover, The PAF-68 specifically initiates $\cdot O_2^-$ rather than singlet oxygen. This makes it have excellent photocatalytic ability even in low oxygen concentration like the room air atmosphere. In addition, in contrast to traditional POP photocatalyst, PAF-68 is a metal-free photocatalyst, which has the advantages of stable structure, environmental friendliness and biocompatibility.

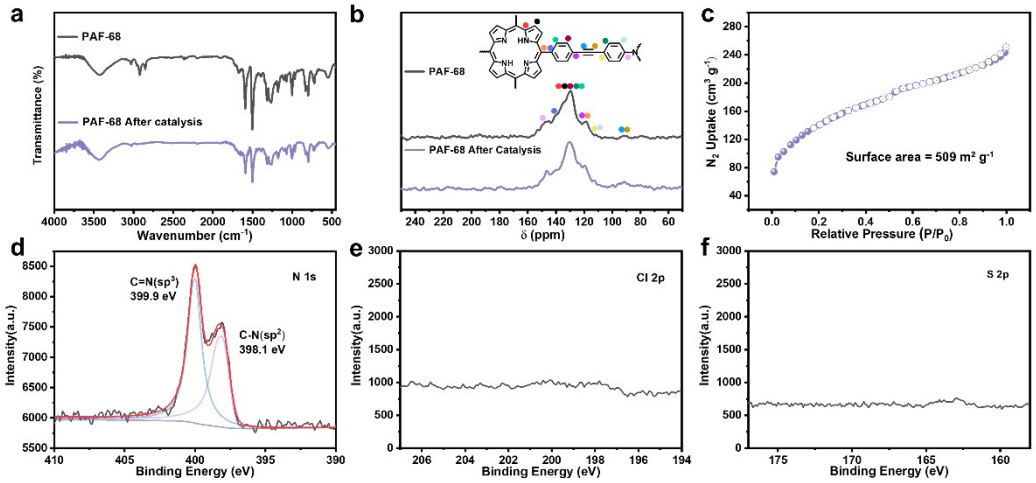

Fig. S22. The (a) FT-IR, (b) solid-state ^{13}C NMR, (c) N_2 adsorption and XPS (d) N 1s (e) Cl 2p (f) S 2p after catalytic cycle of PAF-68.

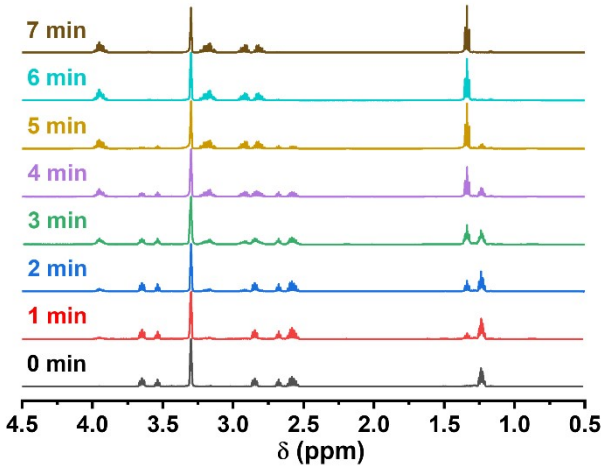

Fig. S23. ^{1}H NMR spectra measured before and after photooxidation in air, using PAF-68 kept at room temperature in room air for a year.

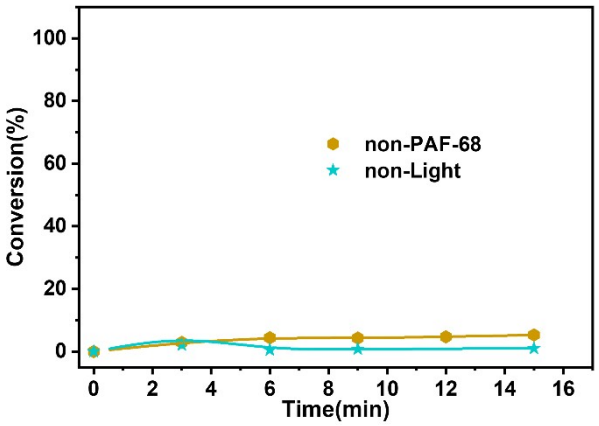

Fig. S24. Control reaction without adding PAF-68 (cyan) and without light (brown).

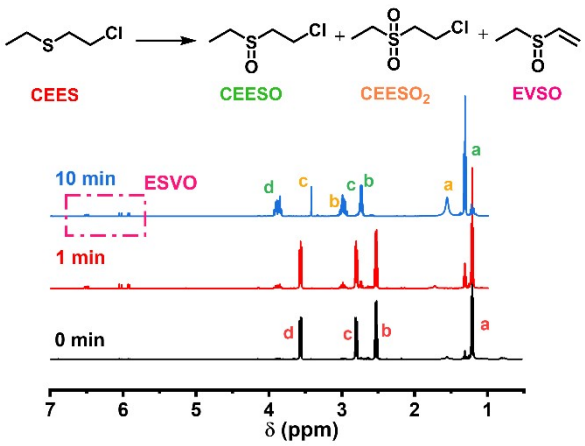

Fig. S25. ^1H NMR spectra of the products for the photooxidation of CEES in $CDCl_3$ after 1 min and 10 min.

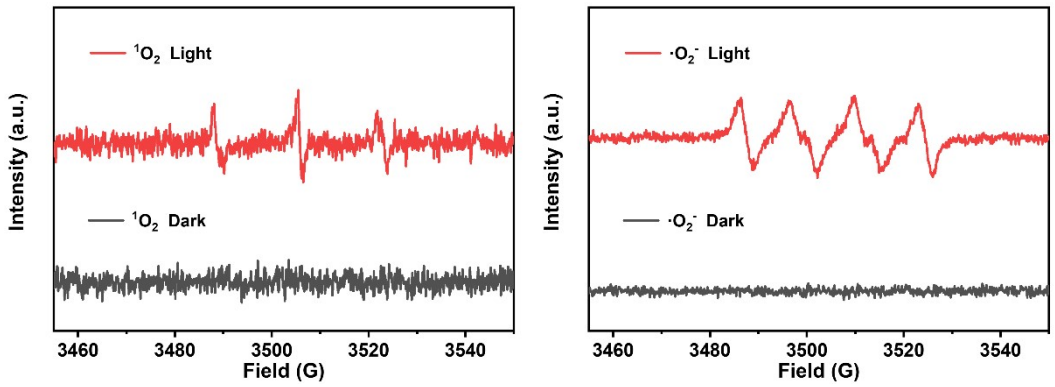

Fig. S26. EPR spectra of PCN-222 mixed with TEMP and DMPO.

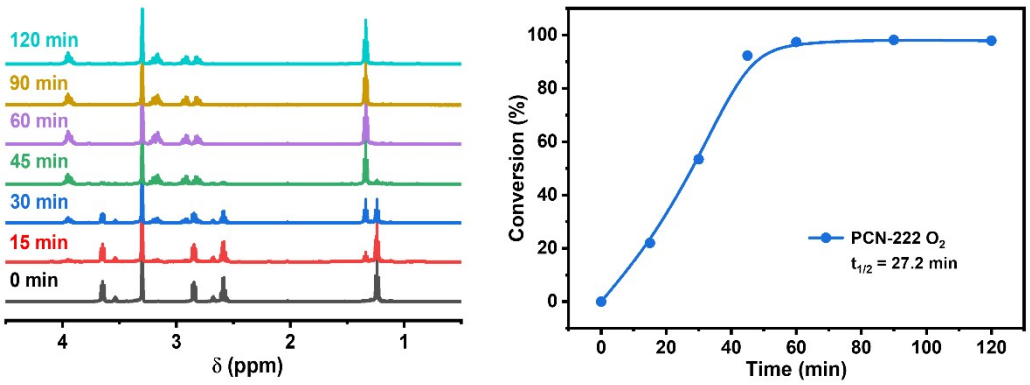

Fig. S27. ^1H NMR spectra and conversion of PCN-222 photocatalysis in pure oxygen.

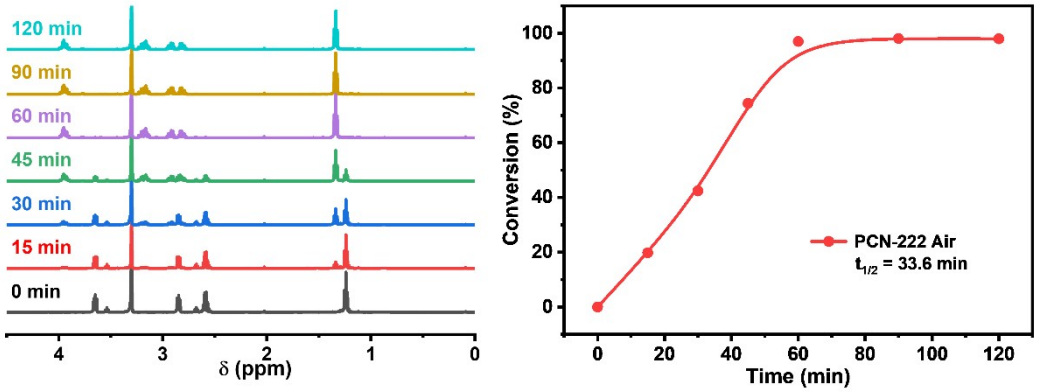

Fig. S28. ^{1}H NMR spectra and conversion of PCN-222 photocatalysis in air.

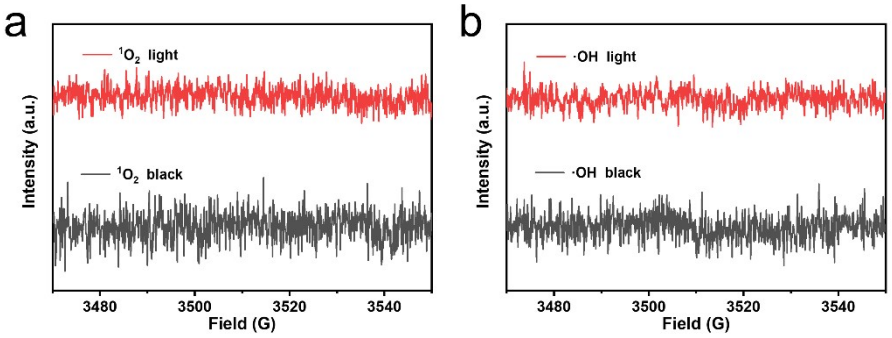

Fig. S29. EPR spectra of PAF-68 mixed with TEMP (a) and DMPO (b).

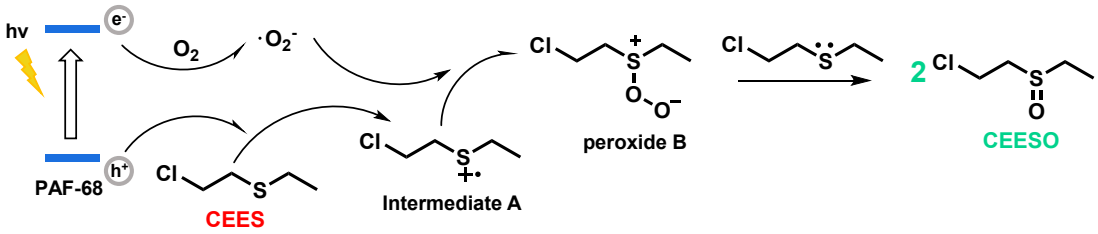

Fig. S30. Proposed reaction pathways for CEES oxidation via $\bullet O_2^-$.

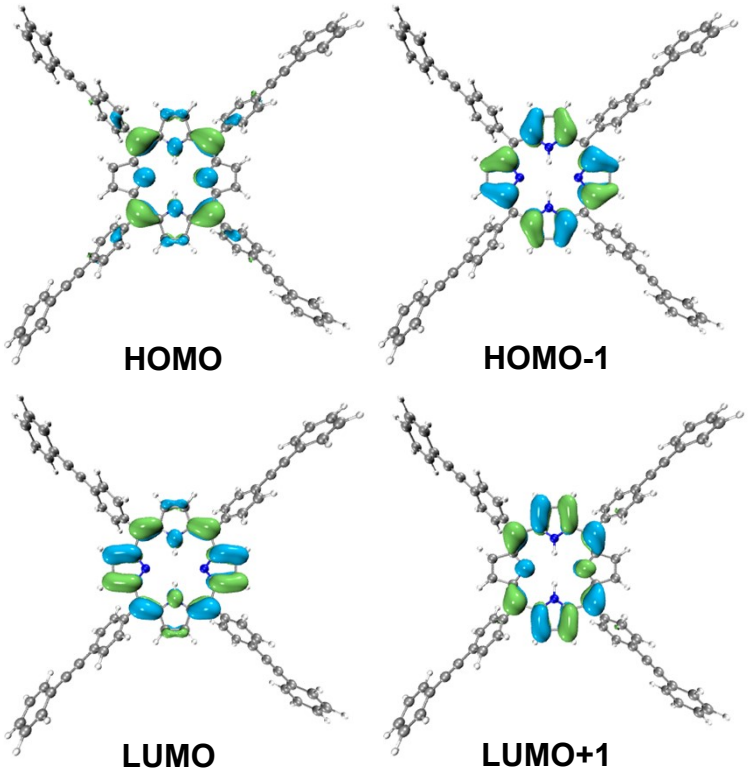

Fig. S31. The frontier orbitals relevant to the excited singlet and triplet states in PAF-68 are calculated.

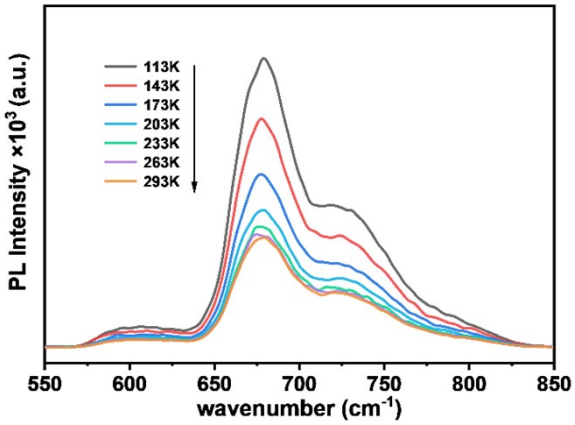

Fig. S32. Temperature-dependent photoluminescence (PL) of PAF-68.

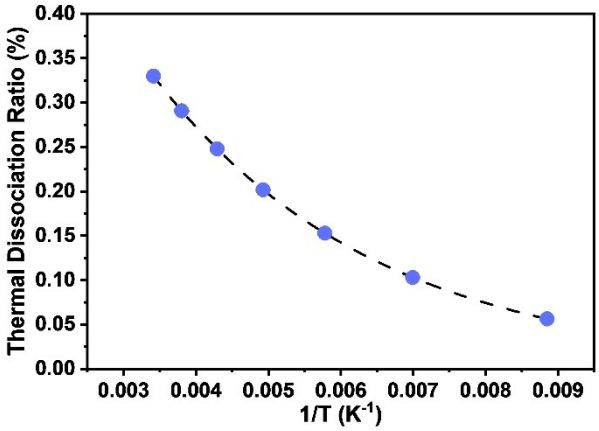

Fig. S33. Exciton dissociation rates in PAF-68 extracted from temperature-dependent PL spectra.

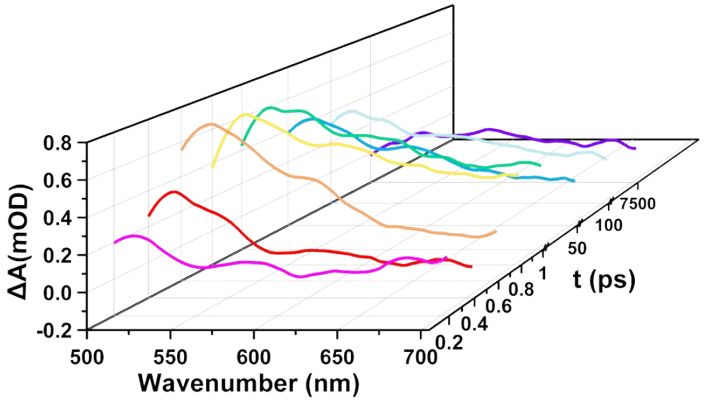

Fig. S34. The corresponding spectra of PAF-68 at selected pump-probe time delays.

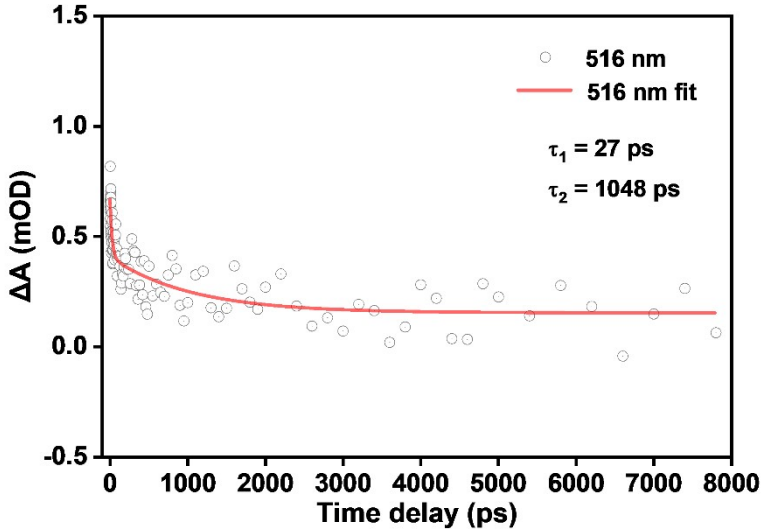

Fig. S35. The kinetics of the characteristic fs-TA absorption bands observed at 516 nm in air at 298 K.

4. Reference

1. Y. Liu, A. J. Howarth, J. T. Hupp and O. K. Farha, *Angew. Chem. Int. Ed.*, 2015, **54**, 9001-9005.
2. M. Cao, R. Pang, Q.-Y. Wang, Z. Han, Z.-Y. Wang, X.-Y. Dong, S.-F. Li, S.-Q. Zang and T. C. W. Mak, *J. Am. Chem. Soc.*, 2019, **141**, 14505-14509.
3. L. Ma, Y. Liu, Y. Liu, S. Jiang, P. Li, Y. Hao, P. Shao, A. Yin, X. Feng and B. Wang, *Angew. Chem. Int. Ed.*, 2019, **58**, 4221-4226.
4. Y. Zhi, Z. Yao, W. Jiang, H. Xia, Z. Shi, Y. Mu and X. Liu, *ACS Appl. Mater. Interfaces*, 2019, **11**, 37578-37585.
5. S. Wang, Q. Sun, W. Chen, Y. Tang, B. Aguila, Y. Pan, A. Zheng, Z. Yang, L. Wojtas, S. Ma and F.-S. Xiao, *Matter*, 2020, **2**, 416-427.
6. D. T. Lee, J. D. Jamir, G. W. Peterson and G. N. Parsons, *Matter*, 2020, **2**, 404-415.
7. A. Atilgan, M. M. Cetin, J. Yu, Y. Beldjoudi, J. Liu, C. L. Stern, F. M. Cetin, T. Islamoglu, O. K. Farha, P. Deria, J. F. Stoddart and J. T. Hupp, *J. Am. Chem. Soc.*, 2020, **142**, 18554-18564.
8. Z.-H. Long, D. Luo, K. Wu, Z.-Y. Chen, M.-M. Wu, X.-P. Zhou and D. Li, *ACS Appl. Mater. Interfaces*, 2021, **13**, 37102-37110.
9. Q. Y. Wang, J. Liu, M. Cao, J. H. Hu, R. Pang, S. Wang, M. Asad, Y. L. Wei and S. Q. Zang, *Angew. Chem. Int. Ed.*, 2022, e20220713.
10. Y. Zhao and D. G. Truhlar, *Theoretical Chemistry Accounts*, 2008, **120**, 215-241.
11. D. Lancet and I. Pecht, *Biochemistry*, 1977, **16**, 5150-5157.
12. M. J. Frisch, G. W. Trucks, H. B. Schlegel, G. E. Scuseria, M. A. Robb, J. R. Cheeseman, G. Scalmani, V. Barone, G. A. Petersson, H. Nakatsuji, X. Li, M. Caricato, A. V. Marenich, J. Bloino, B. G. Janesko, R. Gomperts, B. Mennucci, H. P. Hratchian, J. V. Ortiz, A. F. Izmaylov, J. L. Sonnenberg, Williams, F. Ding, F. Lipparini, F. Egidi, J. Goings, B. Peng, A. Petrone, T. Henderson, D. Ranasinghe, V. G. Zakrzewski, J. Gao, N. Rega, G. Zheng, W. Liang, M. Hada, M. Ehara, K. Toyota, R. Fukuda, J. Hasegawa, M. Ishida, T. Nakajima, Y. Honda, O. Kitao, H. Nakai, T. Vreven, K. Throssell, J. A. Montgomery Jr., J. E. Peralta, F. Ogliaro, M. J. Bearpark, J. J.

Heyd, E. N. Brothers, K. N. Kudin, V. N. Staroverov, T. A. Keith, R. Kobayashi, J. Normand, K. Raghavachari, A. P. Rendell, J. C. Burant, S. S. Iyengar, J. Tomasi, M. Cossi, J. M. Millam, M. Klene, C. Adamo, R. Cammi, J. W. Ochterski, R. L. Martin, K. Morokuma, O. Farkas, J. B. Foresman and D. J. Fox, Gaussian 16 Rev. C.01.*Journal*, 2016.